July 1998 ● NREL/CP-520-23915

Electrical Characterization of CdTe Grain-Boundary Properties from As Processed CdTe/CdS Solar Cells

L.M. Woods, D.H. Levi, V. Kaydanov, G.Y. Robinson, and R.K. Ahrenkiel

Presented at the 2nd World Conference and Exhibition on
Photovoltaic Solar Energy Conversion; 6-10 July 1998; Vienna, Austria

National Renewable Energy Laboratory
1617 Cole Boulevard
Golden, Colorado 80401-3393
A national laboratory of the
U.S. Department of Energy
Managed by the Midwest Research Institute
For the U.S. Department of Energy
Under Contract No. DE-AC36-83CH10093

ELECTRICAL CHARACTERIZATION OF CdTe GRAIN-BOUNDARY PROPERTIES FROM AS PROCESSED CdTe/CdS SOLAR CELLS

L.M. Woods,* D.H. Levi, V. Kaydanov,** G.Y. Robinson,* and R.K. Ahrenkiel
National Renewable Energy Laboratory, 1617 Cole Blvd., Golden, Colorado 80401, USA
*Colorado State University, Ft. Collins, Colorado 80523, USA
**Colorado School of Mines, Golden, Colorado 80401, USA

ABSTRACT: An ability to liftoff or separate the thin-film polycrystalline CdTe from the CdS, without the use of chemical etches, has enabled direct electrical characterization of the *as-processed* CdTe near the CdTe/CdS heterointerface. We use this ability to understand how a back-contact, nitric-phosphoric (NP) etch affects the grain boundaries throughout the film. Quantitative determination of the grain-boundary barrier potentials and estimates of doping density near the grain perimeter are determined from theoretical fits to measurements of the current vs. temperature. Estimates of the bulk doping are determined from high-frequency resistivity measurements. The light and dark barrier potentials change after the NP etch, and the origin of this change is postulated. Also, a variable doping density within the grains of non-etched material has been determined. These results allow a semi-quantitative grain-boundary band diagram to be drawn that should aid in determining more-accurate two-dimensional models for polycrystalline CdTe solar cells.
Keywords: CdTe - 1: Grain Boundary Barrier - 2: Nitric - Phosphoric etch - 3

1. INTRODUCTION

It is generally believed that diffusion of impurities up grain boundaries from the underlying films and substrate greatly affect the electrical properties of the CdTe film during growth and subsequent high-temperature processing of a CdS/CdTe device. Herein, we will make use of an ability to liftoff or separate the post-processed thin-film polycrystalline CdTe from the CdS, SnO_2 and glass substrate, without the use of chemical etches. We use this ability to understand how a back-contact, nitric-phosphoric (NP) etch affects the grain boundaries of the front buried homojunction and postulate the subsequent effects on device operation. A connection was established between the NP etch and the electrical junction, 7.5 microns away, in a recent photoluminescence study [1].

In our study, we will present theory and quantitative determination of the grain boundary barrier potentials, and will estimate the bulk doping, as well as the doping density near the outside of the grain. These properties are determined from measurements of DC current versus temperature, and DC and AC electrical conductivity, and are found as a function of back-contact processing and depth into the film.

These findings will aid in determining more-accurate two-dimensional models of the polycrystalline devices for fully understanding device operation.

2. EXPERIMENTAL CONDITIONS

2.1 Sample Preparation

All samples described herein were processed at the National Renewable Energy Laboratory (NREL). The CdTe film is deposited by close-spaced sublimation (CSS) onto CdS, which is deposited by a chemical-bath solution. The substrate was a bilayer SnO_2-coated Corning 7059 glass. The as-grown CdTe film thickness is about 10 µm. The CdTe/CdS devices receive a high-temperature $CdCl_2$ vapor treatment. At this point, a 30-second NP etch (about 1% nitric acid, 70% phosphoric acid, and 29% water) dip is performed on some samples. All samples are then ion-beam-milled about 250 nm, which removes the conducting Te-rich surface from the samples that were NP etched. Further milling is performed to achieve the total film thickness of 10, 7.5, 5.0, 3.5, and 2.0 µm, to systematically study the effects of the NP etch on the grain boundaries versus depth. The remaining CdTe film is removed or lifted off from the device by using a technique similar to that of von Windheim et al. [2], but developed independently at the National Renewable Energy Lab. for CdTe on CdS. In this manner, smooth films of CdTe formerly in contact with CdS can be made as large as 1.5 cm in diameter. Several parallel strips of gold contacts are then applied by evaporation and by using metal masks. The contacts are 11 mm long and are spaced 0.4 mm apart.

2.2 Measurement Apparatus

Electrical measurements were made using a two-probe method, a heated copper block, temperature controller, and thermocouple for temperature monitoring and feedback. A Keithley 485 picoammeter was used for the DC current measurement that was fully automated with computer control. The AC resistance was measured using HP 4274 and 4275 LCR meters, which together provided a 100-Hz to 10-MHz frequency range. An HP 6825 external power supply provided bias control. A three-point probe method was used to confirm neglible contact resistance.

3. BACKGROUND AND THEORY

It has been shown that polycrystalline material can be modeled, as shown in Fig. 1 [3]. Typically, the grain-boundary resistance dominates the film resistivity, $R_1 >> R_2$. Thus, R_1 dictates the DC conductivity measurement and enables the grain-boundary properties to be studied. A high-frequency measurement of the conductivity effectively shorts out R_1 via C and enables us to measure the intragrain resistance, R_2.

The primary deterrent for determining grain-boundary potentials is the lack of knowledge of the doping density near the grain boundaries. Without this knowledge, one can not easily predict whether the conduction mechanism over the grain boundary is due to drift-diffusion, thermionic, thermally assisted tunneling, or just tunneling. Thus, previous studies report only the conductivity activation energies [2], or assume thermionic emission based on bulk values of the doping density or measurements of *bi*crystal capacitance [4]. We have found that measurement of *poly*crystalline capacitance is unreliable at this point due to geometry considerations. In this report, the conduction mechanism will be determined by analyzing the conductivity temperature dependence. This approach has been used in the past on polycrystalline GaAs [5]. In this study, values of barrier height and doping density are taken from the conduction model that best fits the current temperature dependence.

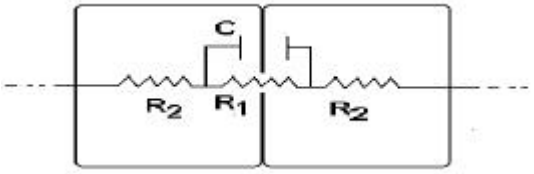

Figure 1: Grain-Boundary Electrical Model with intragrain resistance, R_2, in series with a grain-boundary impedance, R_1 in parallel with C. Typically, $R_1 >> R_2$.

The current-voltage relation for grain boundaries has been developed by Muller [6]. The following voltage dependence for grain boundaries has been determined for small-applied voltages or qV<<2kT, by equating currents into the grain boundary with those exiting the grain boundary:

$$J \cong (2-\gamma) J_0 \left(\frac{qV}{2kT} \right), \qquad (1)$$

where J_0 is the model-dependent portion of the saturation current, V is an estimate of the voltage applied per grain boundary, and γ is the grain-boundary capture coefficient and is a number between 0 and 1. In equation (1), the variation of the Fermi level in the boundary is neglected as it is predicted to be small. Thus, the small applied voltage result with γ=0 is the same current-voltage relation derived for small-applied voltages of a Schottky barrier. Because the current-voltage relation is independent of the conduction mechanism, erroneous estimates of γ and V are not expected to alter the results as to which model fits best.

Crowell and Sze developed a current model for Schottky barriers that combines drift-diffusion theory with thermionic emission theory [7]. The saturation current from this theory can be written as:

$$J_0 = \frac{qN_b}{\frac{1}{\nu_d} + \frac{1}{\nu_r}} \exp\left(-\frac{qV_b}{kT} \right), \qquad (2)$$

where V_b is the grain-boundary barrier height, N_b is the doping in the vicinity of the grain boundary, ν_d is the effective diffusion velocity and is equal to μE_m. E_m is the value of the maximum electric field, which in this case is equal to $(2qN_bV_b/\varepsilon_s)^{1/2}$ for a double depletion region at barrier maximum. Also, ν_r is the "recombination velocity" for carriers thermally emitted over the barrier and is a constant of the material equal to $(kT/2\pi m^*)^{1/2}$. Thus, if ν_r is much lower than ν_d, then the current flow is limited by thermionic emission. Conversely, if ν_d is much lower than ν_r, then the current flow is limited by drift-diffusion. In this equation quantum mechanical reflection of carriers is neglected as well as phonon backscattering and image force barrier lowering. These factors are not expected to appreciably alter V_b, or give order of magnitude differences in N_b, according to the authors.

Crowell and Rideout developed a current model for Schottky barriers that assumes thermally assisted tunneling [8]. This model covers the full range from pure thermionic emission to pure tunneling; however, the approximations used begin to break down at these limits. The saturation current for this model can be written generally as follows:

$$J_0 = \frac{A^* T}{k} \int_0^\infty f_1(E) T(E) f_2(E) dE, \qquad (3)$$

where A* is the Richardson constant, and f_1 and f_2 are the Fermi-Dirac occupancy functions of the left and right-hand side, respectively. T(E) is the transmission probability assuming the WKB approximation, a parabolic potential or uniform doping, a parabolic energy-momentum relationship, and a carrier with energy E. In equation (3), the density-of-states dependence on energy is removed from the integrand and contained within A*. This approximation only becomes non-negligible for carriers with low energy or when tunneling through the bottom of the barrier is dominant. Also, no mixing of valence and conduction band states was taken into account, which can lead to errors if the barrier height is greater than ½ E_g [9]. The validity of this approximation is to be determined.

Padovani and Stratton (P&S) estimated an analytical solution to equation (3) by expanding the transmission probability integral of equation (3) in a Taylor series around the energy, where the number of emitted carriers is maximum [10]. This gives the following saturation current equation for a reverse-biased Schottky barrier:

$$J_0 \cong \frac{A^* T}{k} \sqrt{\pi E_{00}} \sqrt{-qV - E_{vf} + \frac{qV_b + E_{vf} - qV}{\cosh\left[\left(E_{00}/kT \right)^2 \right]}} \; x \exp\left(-\frac{qV_b + E_{vf} - qV}{E_{00} \coth\left(E_{00}/kT \right)} \right), \qquad (4)$$

where V in this case is the applied voltage per grain boundary. and is usually negligible for small-applied voltages. With E_{00} being a constant that is proportional to the square root of N_b and is equal to:

$$E_{00} = \frac{qh}{4\pi} \sqrt{\left(\frac{N_b}{m^* \varepsilon_s} \right)}, \qquad (5)$$

The energy separation between the Fermi level and valence bands, E_{vf} , near the grain boundary, but in the absence of a

potential barrier, can be expressed in terms of E_{00}. The value of E_{00}, or doping density, determines how far up the barrier the peak in thermally assisted emission occurs, and the energy spread of this emission is related to the barrier energy.

4. RESULTS

To confirm the existence of a dominate grain-barrier resistance and the model as shown in Fig. 1, the resistance frequency response was performed on etched and non-etched samples. Fig. 2 shows an example of the resistivity dependence on frequency in the light, and thus, confirms the model. As can be seen from the figure, the resistance is reduced by several orders of magnitude at high frequencies and is indicative of the dominant barrier resistance. Also, the value of high-frequency resistance is nearly constant in all samples. This indicates that the intragrain resistance, or bulk doping, remains unchanged. However, there is a dependence on the low-frequency resistance, or barrier resistance, between etched and non-etched samples.

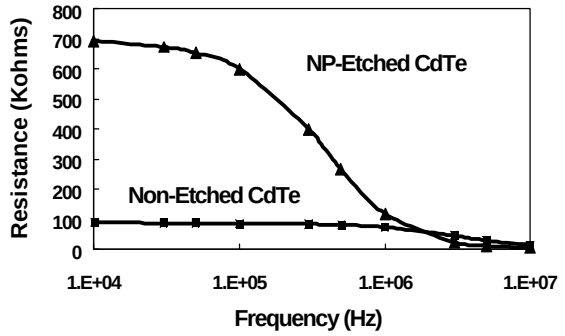

Figure 2: Resistance frequency response of non-etched and NP-etched CdTe under 1-sun illumination. Breakpoint is approx. equal to $(R_1C)^{-1}$.

The barrier potentials, V_b, were determined by measuring the current vs. temperature for each sample and fitting each sample to each conduction model as described earlier. The results of each fit for a typical non-etched sample are shown in Fig. 3. As can be seen from the figure, the thermally assisted tunneling model fits best. It should be noted that the maximum value of N_b was limited to 10^{15} cm^{-3} for drift-diffusion, as at this point $\nu_r \approx \nu_d$. A maximum value was also set for the thermionic emission case of $N_b = 10^{17}$ cm^{-3}, as at this point the effects of tunneling may be significant. If the best fit for thermionic emission went to this maximum, then the data should be fit with the thermally assisted tunneling model. This was the case for the samples herein. The barrier height, V_b, as determined by the thermally assisted tunneling model was 772 meV and E_{00} was 7.9 meV. This barrier height correlates well with values of about 0.8 eV for the valence band offset between an unreacted metal on a "pinned" Fermi level CdTe surface [11]. For comparison, V_b as determined from thermionic emission was 624 meV using the maximum value of N_b. N_b as determined from E_{00} is about $7x10^{17}$ cm^{-3}. Thus, previous studies, which used bulk values for N_b, would yield even lower and more erroneous values for V_b.

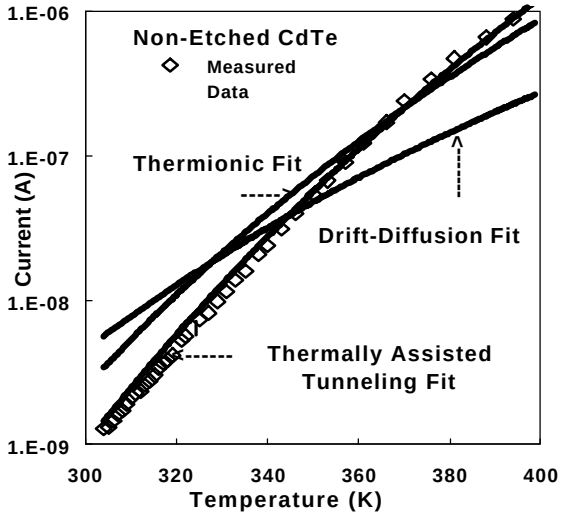

Figure 3: Comparison of fits to current vs. temperature data for different models of conduction.

Similar good fits can be obtained for the NP-etched samples. In this case, the thermionic model fits almost as well as the thermally assisted tunneling model. It was observed that varying the conduction thickness over a couple of orders of magnitude had little effect on the resultant barrier height of about 275 meV. For comparison, a V_b of 302 meV was obtained for the thermionic-only fit and using the maximum N_b value. The thermally assisted tunneling model value of V_b compares well with the value of 0.26 eV for the valence-band offset between evaporated Te on CdTe [11]. It was shown previously that the N-P etch preferentially etches grain boundaries and creates Te-rich grain boundaries [1].

The results of the fit and high-frequency resistance measurements for a non-etched sample allow us to calculate the shape of the band diagram, as seen in Fig. 4:

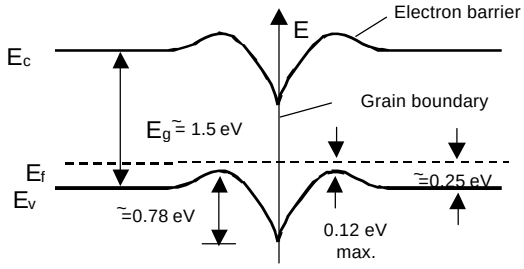

Figure 4: Grain-Boundary Band Diagram of non-etched CdTe. V_b and N_b as determined from thermally assisted tunneling theory fit to current vs. temperature data.

The bulk doping level was estimated to be about $7x10^{14}$ cm^{-3} and was determined from the value of the high-frequency intragrain resistance, device geometry, and a nominal value of 60 cm^2/v-s as the bulk hole mobility in crystalline CdTe. This doping level is about three orders of magnitude less than the doping in the vicinity of the grain boundary and gives rise to a minority-carrier barrier of about 0.12 eV near the potential barrier. However, the spatial extent of this barrier is unknown.

Because it was shown that the NP etch reduces the grain-boundary barrier height, the next step was to determine the

extent of this effect with depth in the sample. Fig. 5 plots each of the NP-etched samples that have also been ion-beam milled to various depths in order to profile the effect. Non-etched, but ion-beam-milled samples were also measured for comparison. Four samples were processed at each film thickness, two non-etched and two NP-etched, and agreement between similarly processed samples was very good.

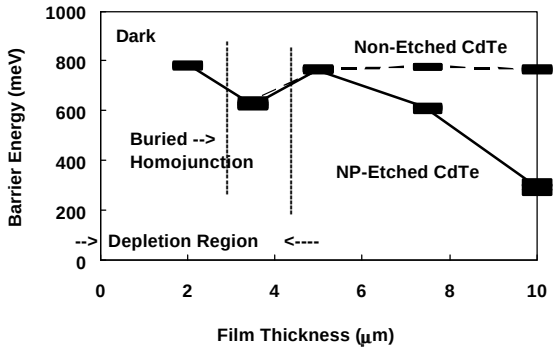

Figure 5: Effect of the NP etch on the CdTe grain-boundary barrier vs. depth. Possible extent of depletion region is shown due to buried homojunction.

From this plot we see that the N-P etch losses its effects after 5 μm of film have been removed. It was later shown that an NP-etched material had a buried homojunction that occurs about 2.5 μm into the film, (thickness = 2.5 μm), as deduced from electron-beam-induced-current (EBIC) measurements. This would deplete the adjacent 1-2 μm and thus possibly affect the result at a film thickness of 5 μm. The results below 5 μm are thus poorly understood at this point. It is also interesting to note that the barrier energy of about 0.6 eV for the film of thickness = 7.5 μm (2.5 μm of material removed) correlates well with the valence-band offset of about 0.59 eV between CdTe and a thin layer (t < 50 Å) of evaporated Te [11].

The 10-μm-thick, lightly milled samples were periodically remeasured over six months in room atmosphere to determine the stability of the barrier-reducing etch. The barrier heights asymptotically degraded (increased) quickly in the first couple of months, but then stabilized to an average value of 350 meV. This degradation is most likely due to oxidation of the tellurium in the grain boundaries. The oxidation of tellurium has been shown in a previous study using X-ray photoelectron spectroscopy [11], and results from that study indicate that it is likely that the NP-etched samples underwent a great deal of oxidation before the first samples were measured. A change in barrier height between 275 meV and 350 meV can increase the barrier resistance by an order of magnitude for devices relying on the NP etch to provide an interface layer for low-resistance back contacts. The non-etched, 10-μm samples were also remeasured for comparison, but their barrier heights were unchanged during the six months.

5. DISCUSSION AND CONCLUSIONS

Measurements of the grain-boundary barrier heights correlate with other measurements of valence-band offsets from a previous study. This previous study postulated that the N-P etch reduced the barrier height by creating a p-type tellurium layer to compensate the n-type defects at the grain boundary [11]. Also shown was a variable grain doping level, with increasing doping near the grain boundary of several orders of magnitude when compared to the bulk concentration. This information has allowed a detailed development of the grain-boundary band diagram, which predicts a minority-carrier or conduction-band barrier due to the variable doping. We postulate that if this layer is wider than electron mean free path length, then this layer could act to reflect the minority carriers before the grain boundary, and thus, temper the grain-boundary barrier effects on minority-carrier recombination. Lifetimes measured by time-resolved photoluminescence and solar cell J_{sc} measurements [12] corroborate this and appear to be unchanged by the NP etch. Finally, it was shown that the effects of the N-P etch are initially unstable and could result in severe increases in the back-contact series resistance of devices.

ACKNOWLEDGEMENTS

The authors would like to thank the following NREL employees: David Albin for growing the samples; Yoxa Mahathongdy for performing the $CdCl_2$ treatment; Anna Duda and Aaron Szalaj for aiding in the metal evaporation; and Tim Gessert for performing the ion-beam milling. This project was funded by the U.S. Department of Energy under contract DE-AC36-83CH10093.

REFERENCES

[1] D.H. Levi, et al., *Twenty-Sixth IEEE PVSC*, (1997).
[2] J. von Windheim, I. Renaud, and M. Cocivera, *J. Appl. Phys.*, **67**,(9) 1990.
[3] D.P. Snowden and A. M. Portis, *Phys. Rev.*, **120**,(6) 1960.
[4] T.P. Thorpe, Jr., A.L. Fahrenbruch, and R.H. Bube, *J. of Appl. Phys.*, **60**(10), p. 3622, (1986).
[5] C.H. Seager and G.E. Pike, *Appl. Phys. Lett.*, **40**(6), pg. 471, (1982).
[6] R.K. Muller, *J. of Appl. Phys.*, 32(4), p. 635, (1961).
[7] C.R. Crowell and S.M. Sze, *Solid-St. Electron.*, **9**, p. 1035, (1966).
[8] C.R. Crowell and V.L. Rideout, *Solid-St. Electron.*, **12**, p. 89, (1969).
[9] J.W. Conley and G.D. Mahan, *Phys. Rev.*, **161**(3), p. 161, (1967).
[10] F.A. Padovani and R. Stratton, *Solid-St. Electron.*, **9**, p. 695, (1966).
[11] D.W. Niles, X. Li, P. Sheldon, and H. Hochst, *J. of Appl. Phys.*, **77**(9), p. 4489, (1995).
[12] Xiaonan Li, private communication, 1997.